A PK/PD Analysis of Circulating Biomarkers and Their Relationship to Tumor Response in Atezolizumab-Treated non-small Cell Lung Cancer Patients

Ida Netterberg[1,2], Chi-Chung Li[3], Luciana Molinero[3], Nageshwar Budha[3], Siddharth Sukumaran[3], Mark Stroh[3], E. Niclas Jonsson[2] and Lena E. Friberg[1,2]

To assess circulating biomarkers as predictors of antitumor response to atezolizumab (anti-programmed death-ligand 1 (PD-L1), Tecentriq) serum pharmacokinetic (PK) and 95 plasma biomarkers were analyzed in 88 patients with relapsed/refractory non-small cell lung cancer (NSCLC) receiving atezolizumab i.v. q3w (10–20 mg/kg) in the PCD4989g phase I clinical trial. Following exploratory analyses, two plasma biomarkers were chosen for further study and correlation with change in tumor size (the sum of the longest diameter) was assessed in a pharmacokinetic/pharmacodynamic (PK/PD) tumor modeling framework. When longitudinal kinetics of biomarkers and tumor size were modeled, tumor shrinkage was found to significantly correlate with area under the curve (AUC), baseline factors (metastatic sites, liver metastases, and smoking status), and relative change in interleukin (IL)-18 level from baseline at day 21 ($RCFB_{IL\text{-}18,d21}$). Although AUC was a major predictor of tumor shrinkage, the effect was estimated to dissipate with an average half-life of 80 days, whereas $RCFB_{IL\text{-}18,d21}$ seemed relevant to the duration of the response.

Study Highlights

WHAT IS THE CURRENT KNOWLEDGE ON THE TOPIC?

☑ Several CIT checkpoint inhibitors have been approved for cancer treatment, but response to treatment is highly variable between patients. There is an unmet need for minimally invasive early predictive biomarkers of clinical outcome to inform clinical practice and drug development decisions.

WHAT QUESTION DID THIS STUDY ADDRESS?

☑ How can a pharmacometric modeling framework be used to identify early predictive biomarkers of response to a cancer immunotherapy, atezolizumab?

WHAT DOES THIS STUDY ADD TO OUR KNOWLEDGE?

☑ The atezolizumab AUC and elevation of IL-18 on day 21 together were early and significant predictors of tumor shrinkage. AUC was a primary driver of the initial response, whereas IL-18 best predicted the duration of the antitumor response.

HOW MIGHT THIS CHANGE CLINICAL PHARMACOLOGY OR TRANSLATIONAL SCIENCE?

☑ IL-18 is a potential early biomarker of atezolizumab antitumor efficacy useful to inform dose and patient selection strategy in clinical development and practice. We propose a quantitative framework that can be integrated with biomarker research and discovery to enable personalized medicine for cancer treatment.

Cancer immunotherapy (CIT) has become a new pillar of oncology treatment.[1–3] In contrast to traditional cancer drugs, these agents aim to stimulate the patient's pre-existing immune response against tumor cells at different stages of the cancer immunity cycle.[4] Immune checkpoint blockade with anti-cytotoxic T lymphocyte-associated antigen 4 (CTLA-4) and anti-programmed cell death 1 (PD-1)/programmed death-ligand 1 (PD-L1) antibodies either as monotherapy or in combination with a variety of agents, for example, can elicit a durable clinical antitumor response in a subset of patients. However, individual responses to CIT vary widely, reflecting the interpatient heterogeneity in immune and disease status, as well as the involvement of various immune escape mechanisms.[5,6]

I. Netterberg and C. C. Li shared first authorship.

[1]Department of Pharmaceutical Biosciences, Uppsala University, Uppsala, Sweden; [2]Pharmetheus AB, Uppsala, Sweden; [3]Department of Clinical Pharmacology, Genentech, South San Francisco, California, USA. Correspondence: Chi-Chung Li (li.chichung@gene.com)

Received 27 April 2018; accepted 15 July 2018; advance online publication 4 September 2018. doi:10.1002/cpt.1198

In the era of personalized medicine in oncology, there remains a high unmet need for the identification of minimally invasive, predictive biomarkers to provide an early assessment of the individual patient's likelihood of benefiting from a particular treatment and thereby optimize treatment decisions for the patient. Biomarker research aimed at finding predictive and prognostic biomarkers to guide patient selection for immune checkpoint inhibitor therapies led to the development of companion diagnostics to assess baseline expression of PD-L1 on tumor and immune cells.[3,6–8] Although patients with PD-L1-positive cells that exhibit an inflammatory phenotype[9,10] are more likely to respond to anti-PD-1/PD-L1 therapies, PD-L1 staining alone does not fully explain the response heterogeneity.[2,6,11,12] Tumor mutational load has shown to be correlated with better response to CIT as a result of enhanced immunogenicity to neoantigens and epitope spreading;[13,14] however, assessment of tumor mutational load currently requires a valid tumor biopsy sample, which can be challenging to patients and the care team.

Peripheral immune biomarkers, such as cytokine levels and prevalence of different immune cell subtypes, present a potential opportunity to monitor real-time changes in patients' immune response to CIT treatment. However, previous reports suggest that, although marked systemic elevations were observed in the levels of several peripheral biomarkers following anti-PD-L1 treatments, these biomarkers did not correlate to tumor response.[6] For ipilimumab (anti-CTLA-4 Yervoy), several serum biomarkers, such as baseline lactate dehydrogenase, vascular endothelial growth factor, and C-reactive protein (CRP) were identified as significant predictors of overall survival.[15–17] However, these biomarkers were baseline pretreatment values and did not reflect the proximal mechanism of action of the drug. Other immunologically relevant markers, such as frequency of $CD4^+ICOS^{hi}$ T cells, eosinophil counts, and soluble CD25 (interleukin (IL)-2 receptor alpha chain), have also been previously reported to be associated with clinical response to ipilimumab.[18–20] However, these analyses did not fully leverage the longitudinal information of the biomarker and tumor data collected and, thus, did not offer insights into the response dynamics at a patient level. In addition, drug exposure was not accounted for in most of these analyses. In addition, although Chatterjee *et al.*[21] reported the development of a longitudinal tumor growth inhibition (TGI) model for pembrolizumab (anti-PD-1, Keytruda) that accounted for drug exposure, no biomarkers were evaluated in that study.

Integrated pharmacokinetic/pharmacodynamic (PK/PD) modeling frameworks have previously been proposed in oncology,[22] both for non-small cell lung cancer (NSCLC)[23] and other tumor types,[24–29] to aid in clinical response characterization and drug development decisions. As anticancer immunity is a complex and dynamic process, the characterization of drivers of treatment response requires a multifactorial approach. Here, we report the successful development of a PK/PD tumor-modeling framework for atezolizumab and its application to evaluating circulating predictive biomarkers in the context of pharmacokinetic (PK) and potential baseline predictive and prognostic factors. Longitudinal biomarker and tumor size information were incorporated into the model to take advantage of the full timecourse of data collected in the PCD4989g phase I clinical trial.[6]

RESULTS

Patients and data

Serum atezolizumab PK and 95 plasma biomarkers (**Table S1**) were analyzed in 88 patients with relapsed/refractory NSCLC who received i.v. q3w doses of atezolizumab from 10, 15, and 20 mg/kg or 1,200 mg in the phase Ia PCD4989g trial (NCT01375842).[6] Eight of the 95 biomarkers assessed met one or both of the following criteria: statistically significant changes from baseline levels or biological relevance as a proximal marker to the mechanism of action of atezolizumab. These eight biomarkers were CRP, CD40, intercellular adhesion molecule 1 (ICAM-1), interferon-inducible T-cell alpha chemoattractant (ITAC), IL-18, IL-8, vascular cell adhesion molecule 1 (VCAM-1), and proliferating and activated $CD8^+$ T cells expressing HLA-DR and ki67 ($T_{CD8,prolif/activ}$). The total number of observations for each biomarker ranged from 413–458, except for $T_{CD8,prolif/activ}$, where 185 measurements were collected (**Table S2**). The median duration of tumor assessment for the patients with NSCLC was 18 weeks, with a range from 0 (4 patients with baseline assessment only) to 153 weeks. All patients were included in the analysis.

The median tumor size (sum of the longest diameters (SLDs)) was 5 cm at baseline, increased modestly following the first two tumor scans (at 6 and 12 weeks), reflecting dropout of nonresponders, and decreased and remained lower than baseline for a sustained period of time (**Figure 1a**). Following atezolizumab administration, the levels of the selected biomarkers typically increased during the first treatment cycle with an observed peak at approximately day 21, followed by a reduction in concentration in later cycles (**Figure 2**).

Initial biomarker assessment and selection for PK/PD-tumor modeling

Of the eight prioritized biomarkers, ITAC and IL-18 showed apparent dose-exposure relationships (**Figure 2**), allowing exploration of dose/exposure-response relationships. Furthermore, baseline concentrations of these markers were not correlated to baseline tumor size, suggesting changes in these markers were not simply downstream effects of alterations in tumor burden. Both ITAC and IL-18 were previously reported as pharmacodynamic (PD) biomarkers following atezolizumab treatment.[6] Interestingly, the timecourse for ITAC was distinct from the other biomarkers and remained elevated after six cycles of treatment, whereas other biomarkers tended to return to baseline by cycle six. Plotting the biomarker change from baseline (CFB) values against tumor size change revealed a potential correlation for four biomarkers (ITAC, IL-18, IL-8, and VCAM-1), although this was difficult to accurately assess given the variability of the data and patient dropouts during the trial (**Figure S1**). Although $T_{CD8,prolif/activ}$ was a biologically interesting biomarker with a pronounced response post-treatment, the data were too sparse to include in PK/PD tumor modeling. Taken together, IL-18 and ITAC were identified as proximal, independent PD biomarkers and selected for further evaluation.

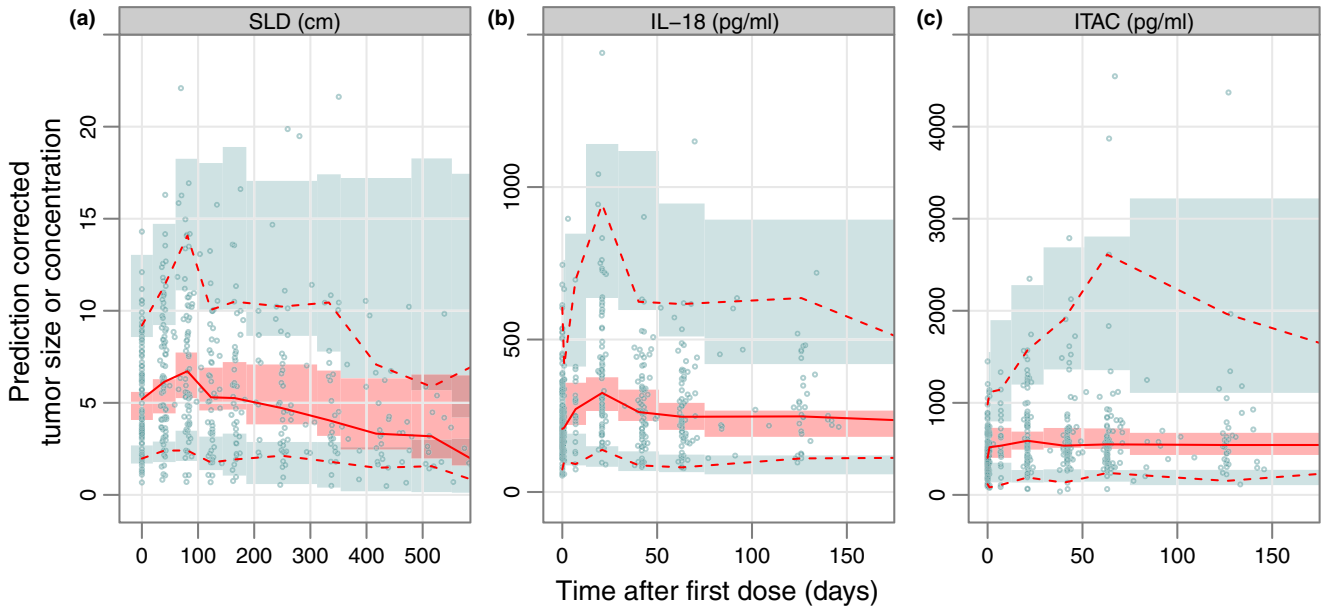

Figure 1 Prediction corrected visual predictive checks (pcVPCs) of timecourse for (**a**) tumor size (sum of the longest diameters (SLDs)), (**b**) interleukin-18 (IL-18), and (**c**) interferon-inducible T-cell alpha chemoattractant (ITAC). The *x* axes are limited to 175 days after first dose for the biomarker pcVPCs and to 585 days after first dose for the tumor growth inhibition (TGI) pcVPC. The dashed lines represent the observed 10th and 90th percentiles for tumor SLD and the 2.5th and 97.5th percentiles for IL-18 and ITAC. Solid lines represent median values. The shaded areas are the 95% confidence intervals of the corresponding percentiles computed from the simulated datasets (N = 500). The dots are observed biomarker concentrations and SLD assessments.

PK model for atezolizumab

A two-compartment PK model was developed based on data from the PCD4989g trial and used for *post hoc* estimates of individual PK values. The model adequately described the data as assessed by prediction-corrected visual predictive checks (pcVPCs) stratified by dose level (**Figure S2**). The model parameters are summarized in **Table S3** and are generally consistent with the values recently reported by Stroh *et al.*[30]

Biomarker models

An indirect-response (IDR) model best described both the IL-18 and ITAC data. Model fit was improved ($P < 0.001$) by inclusion of a pool compartment with a linear relationship describing stimulation of the first-order transfer rate from the precursor pool to the circulating compartment (k_{rel}) by atezolizumab concentration. The inclusion of an effect compartment accounting for the delay of onset of IL-18 significantly improved the model fit ($P < 0.001$) and the VPC for IL-18 but not for ITAC ($P > 0.05$). The pcVPCs for the final IL-18 and ITAC models showed no major model misspecification (**Figure 1b,c**), and parameters were estimated with reasonable precision (**Table 1**).

Tumor growth inhibition model

The tumor size dynamics were best described by the TGI model proposed by Claret *et al.*[31] but with a constant growth rate (R_{growth}) instead of an exponential rate (objective function value Δ(OFV) = 6.4). The tumor shrinkage was best described by a linear function of individual cycle-specific areas under the PK curve ($AUC_{cycle\ n}$), yielding a lower OFV compared to a function of dose (ΔOFV of 5.1) or to a dose-independent rate constant (ΔOFV of 27.0). The OFV was approximately eight units higher when individual first-cycle AUC (AUC_{cycle1}) was used instead of $AUC_{cycle\ n}$. A maximum effect (E_{max}) model for $AUC_{cycle\ n}$ did not provide a significantly better fit.

When tested alone, neither of the investigated biomarker variables (IL-18 and ITAC) fit the data as well as $AUC_{cycle\ n}$ (**Table S4**). However, when relative CFB at day 21 for either IL-18 (relative change from baseline $(RCFB)_{IL\text{-}18,d21}$) or ITAC ($RCFB_{ITAC,d21}$) was included on top of $AUC_{cycle\ n}$, the model fit improved significantly (ΔOFV = 44.2 and 38.9, respectively). The combination of $AUC_{cycle\ n}$ and $RCFB_{IL\text{-}18,d21}$ seemed to best predict tumor size, compared to AUC alone, IL-18 alone, ITAC alone, AUC + ITAC, or all three combined (AUC + IL-18 + ITAC). The timecourse of IL-18 was evaluated but determined to not be a better predictor of the tumor response than $RCFB_{IL\text{-}18,d21}$ (data not shown). The inclusion of an exponentially diminishing $AUC_{cycle\ n}$ effect resulted in a significantly better model fit (ΔOFV of 74).

The rate of tumor size changes (dSLD/dt) for the final TGI model is given in Eq. 1:

$$\frac{dSLD}{dt} = R_{growth} - (K_{Shr,Drug} \cdot AUC_{cycle\ n} \cdot e^{-\lambda_{Drug} \cdot t} + K_{Shr,IL\text{-}18} \cdot RCFB_{IL\text{-}18,d21}) \cdot SLD \quad (1)$$

where $K_{Shr,Drug}$ and $K_{Shr,IL\text{-}18}$ are the tumor shrinking rate constants related to drug exposure and IL-18, respectively, and λ_{Drug} is the rate constant for reduced effect of AUC on tumor shrinkage with time. A reduction in the IL-18 effect over time was investigated but did not provide a better fit. A schematic representation of the final modeling framework (i.e., PK, IL-18, and tumor size) is shown in **Figure 3**.

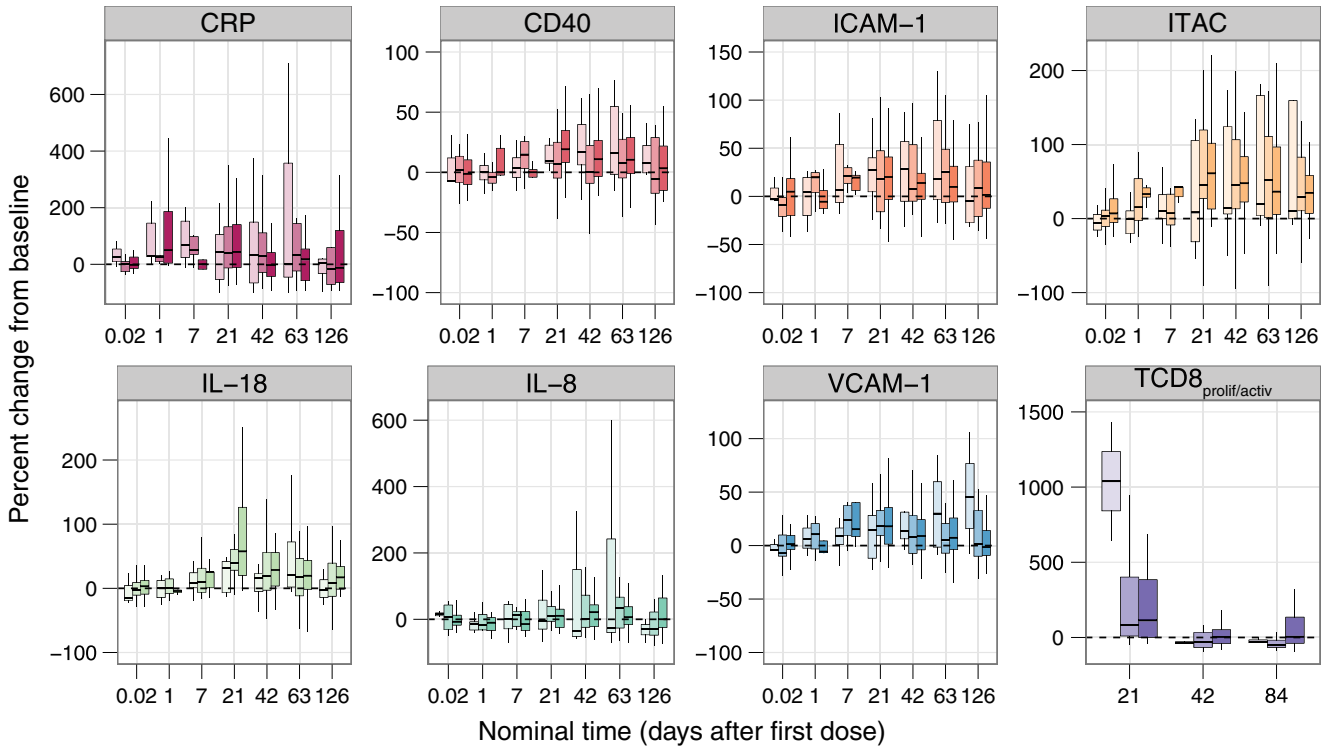

Figure 2 Boxplots of the observed relative change from baseline (RCFB) of eight selected biomarkers vs. protocol-specified nominal time after first dose. The plots are grouped by the protocol-specified nominal dose where the light, medium, and dark boxes represent doses of 10, 15, and 20 mg/kg, respectively. (Data observed following dosing at 1 mg/kg are not shown.) Observations from patients receiving fixed doses of 1,200 mg were assigned to the closest approximates of dose levels in mg/kg (n = 5 assigned to the 15 mg/kg group and n = 2 assigned to the 20 mg/kg group). The upper and lower hinges of the boxes represent the 75th and 25th percentiles, respectively. Upper and lower ends of the whiskers correspond to the 75th percentile+1.5·interquartile range (IQR) and 25th percentile-1.5·IQR, respectively. No outliers are shown. The dashed line indicates no RCFB. CRP, C-reactive protein; CD40, CD40 antigen; ICAM-1, intercellular adhesion molecule 1; ICD, immunogenic cell death; ITAC, interferon-inducible T-cell alpha chemoattractant; IL-18, interleukin 18; IL-8, interleukin 8; VCAM-1, vascular cell adhesion molecule 1; $T_{CD8,prolif/activ}$, activated and proliferating CD8 T cells.

Three covariate-parameter relationships were identified: the number of metastases at baseline and SLD_0 ($\Delta OFV = 21.5$), presence of baseline liver metastases and R_{Growth} ($\Delta OFV = 12.4$), and smoking status and $K_{Shr,Drug}$ (never vs. current/former, $\Delta OFV = 11.2$). For patients with two or fewer metastases at baseline, the typical SLD_0 was 4.8 cm, whereas for patients with more than two metastases, the corresponding value was 9.1 cm. R_{Growth} was nearly 10-fold higher for patients with liver metastases at baseline, compared to patients without (0.16 vs. 0.017 cm/week, respectively). $K_{Shr,Drug}$ approached zero in patients who had never smoked and was set to 0 in the final model.

No statistically significant relationship was found between baseline expression of PD-L1, as assessed by immunohistochemistry of immune cells and immunohistochemistry of immune tumor cells on any of the model parameters. The distribution of PD-L1 expression levels across the patient population is summarized in **Table S5**.

The baseline hazard (h_0) for dropout was described by a constant hazard, and the model-predicted change from tumor size at baseline was a significant predictor in the hazard function ($P < 0.05$). A pcVPC of the final TGI model, together with the dropout model, is presented in **Figure 1** and reveals good fit of the model to the data. All parameter estimates are presented in **Table 1**.

Simulations based on the final TGI model

Following administration of 1,200 mg atezolizumab, the TGI model predicts a sustained antitumor response with no tumor regrowth up to ~27 weeks (nadir of tumor size) followed by a slow return to the tumor size baseline by 89 weeks postdose for an individual with a typical AUC and $RCFB_{IL\text{-}18,d21}$ of 5,600 mg/l*day and 0.43, respectively, corresponding to the medians in the dataset (**Figure 4**). The $AUC_{cycle\ n}$-related effect played a dominant role in early tumor shrinkage, resulting in deeper tumor reduction with higher $AUC_{cycle\ n}$, but the effect dissipated with an estimated average half-life of 80 days. The effect of $RCFB_{IL\text{-}18,d21}$ on tumor shrinkage became more prevalent in later cycles of atezolizumab treatment and seemed to play an important role in the duration of the antitumor response to atezolizumab.

DISCUSSION

To our knowledge, this is the first literature on an integrated pharmacometric framework to evaluate predictive circulating biomarkers for CIT agents in the context of known or investigational baseline prognostic and predictive factors. Using this framework, we further elucidated the relationship between drug exposure ($AUC_{cycle\ n}$) and (i) the initial magnitude of the antitumor response, a direct AUC-related effect, and (ii) the duration of

Table 1 Final parameter estimates and relative standard errors for the interleukin 18 (IL-18), interferon-inducible T-cell alpha chemoattractant (ITAC), dropout and tumor growth inhibition (TGI) models

Parameter[a]	Typical value (RSE, %)[b]	IIV, CV% (RSE, %)
IL-18 model		
R_{in} (pg/mL/day)	23.0 (12)	—
k_{out} (day^{-1})	0.106 (13)	47 (8.7)
$Pool_0$ (pg/mL)	499 (18)	78 (18)
Slope (mL/μg)	0.168 (26)	80 (26)
k_{e0} (day^{-1})	$4.36 \cdot 10^{-3}$ (25)	—
Residual error (%)	22.3 (2.5)	—
ITAC model		
R_{in} (pg/mL/day)	3.07 (24)	48 (10)
k_{out} (day^{-1})	$7.91 \cdot 10^{-3}$ (23)	—
$Pool_0$ (pg/mL)	271 (20)	115 (15)
Slope (mL/μg)	0.0599 (35)	—
Proportional residual error (%)	28.3 (3.9)	—
Additive residual error (pg/mL)	51.8 (15)	—
TGI model		
SLD_0 (cm)	4.75 (11)	62 (8.3)
R_{Growth} (cm/week)	0.0169 (17)	93 (17)
$K_{Shr,Drug}$ (l/mg/day/week)	$2.75 \cdot 10^{-6}$ (23)	124 (21)
λ_{Drug} ($week^{-1}$)	0.0609 (8.7)	—
$K_{Shr,IL\text{-}18}$ (1/(% week))	0.00282 (14.1)	181 (24)
$\theta_{Rgrowth\text{-}LiverMets}$	8.48 (8.5)	—
$\theta_{SLD0\text{-}Mets}$	0.927 (27)	—
$\theta_{KShr,Drug\text{-}Non\text{-}Smoking}$	0 fixed	—
Residual error (%)	13.4 (2.1)	—
Dropout model		
h_0 ($week^{-1}$)	0.0306 (1.8)	
B	1.56 (8.8)	

CV%, coefficient of variation; IIV, interindividual variability; IL-18, interleukin-18; ITAC, interferon-inducible T-cell alpha chemoattractant; RSE, relative standard error; SLD, sum of the longest diameter; TGI, tumor growth inhibition.

[a]R_{in}, zero-order input rate; k_{out}, first-order fractional turn-over rate; $Pool_0$, baseline concentration in the pool compartment; Slope, linear drug effect; k_e, first-order effect compartment rate constant; SLD_0, baseline sum of longest diameters; R_{Growth}, zero-order tumor growth rate; $K_{Shr,Drug}$, rate constant for tumor shrinkage related to drug area under the curve (AUC) in former or current smokers; λ_{Drug}, rate constant for reduced effect of AUC on tumor shrinkage; $K_{Shr,IL\text{-}18}$, rate constant for tumor shrinkage related to IL-18; $\theta_{Rgrowth\text{-}LiverMets}$, describes the fractional change in R_{Growth} $(1 + \theta)$ for patients with liver metastases at baseline; $\theta_{SLD0\text{-}Mets.}$, describes the fractional change in SLD_0 $(1 + \theta)$ for patients with more than two metastases at baseline; $\theta_{KShr,Drug\text{-}Non\text{-}Smoking}$ describes the rate constant for tumor shrinkage related to drug AUC in nonsmokers; h_0, baseline hazard; β, parameter relating the tumor size to dropout. [b]The RSEs related to the PK model were computed based on the NONMEM variance covariance matrix (sandwich matrix). For the biomarker, TGI and dropout models, the RSEs were computed based on the NONMEM variance covariance matrix (S matrix).

that response, an IL-18-related effect estimated by $RCFB_{IL\text{-}18,d21}$, which reflects an "indirect" drug effect (**Figure 4**). Both AUC and $RCFB_{IL\text{-}18,d21}$ are easily measurable and available shortly after treatment begins. These metrics could be used early in treatment to project the potential for a long-term antitumor response. Patient-level PK and IL-18 values could further be used to inform individualized dosing or treatment strategies.

The model predicted a sustained antitumor response followed by tumor regrowth for a typical patient. The potential mechanisms of resistance in patients who responded and then progressed include upregulation of additional inhibitory checkpoints, downregulation of major histocompatibility complex class I molecules on tumor cells, and development of an immunosuppressive tumor microenvironment.[5,32] Although the modeling and simulations conducted here were not designed to predict the clinical duration of response as defined by Response Evaluation Criteria in Solid Tumors (RECIST) version 1.1, and, hence, a direct comparison to clinical duration of response is not possible, the model predicted a sustained tumor size reduction for a typical patient up to 89 weeks following 1,200 mg atezolizumab treatment. A sustained antitumor effect was also observed in the phase II POPLAR clinical trial, where the median duration of response was 14.3 months in patients with NSCLC following 1,200 mg atezolizumab treatment.[33]

IL-18 plays an important role in the production of interferon-γ from activated T cells[34] and has previously been identified as a PD marker following atezolizumab treatment.[6] In the phase I study data used in this analysis, circulating levels of IL-18 were transiently elevated and then rapidly declined after the first treatment cycle. This pattern may reflect initial T-cell activation in the periphery, followed by localization to the tumor, and, thus, serve as a mechanistically relevant early indicator of a response to treatment. Although other biomarkers, including interferon-γ, IL-2, and IL-6, are also relevant to T-cell biology, they did not show statistically significant changes from baseline upon atezolizumab treatment. The timecourse of reduction in tumor size was much more sustained than the transient increase in IL-18, indicating the continued antitumor response at the site of action in tumor tissues following the initial peripheral T-cell activation.

One of the key goals for future immunotherapy strategy is to "raise the tail" of the survival curve.[35] Our findings underscore the relevance of an early immunological biomarker response to the overall survival benefit and its potential utility as an early readout to inform dose and treatment decisions in drug development and clinical practice. The analyses performed by Bruno *et al.*[36] indicate the correlation of tumor growth rate (K_{growth}) estimated by TGI models as a good predictor of survival. Future extensions of this framework may, therefore, include investigation of TGI and IL-18 and relationship to survival following treatment with atezolizumab or other CIT agents.

Among all the potential baseline prognostic factors screened, number of baseline metastatic sites, patients with liver metastases at baseline, and patient smoking status were statistically significant covariates of SLD_0, R_{Growth}, and $K_{Shr,Drug}$, respectively. The findings are consistent with the expectation that more metastases are generally correlated with larger tumor size and

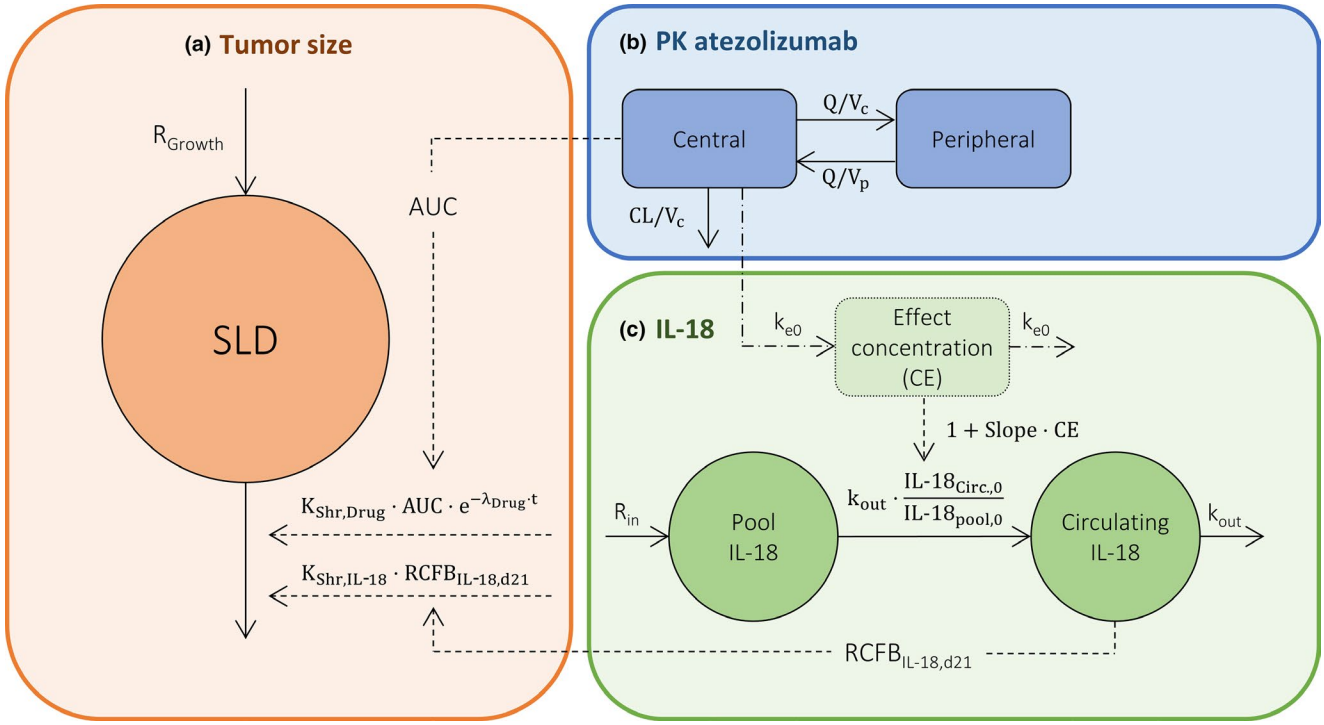

Figure 3 A schematic representation of (**a**) tumor size, (**b**) atezolizumab pharmacokinetic (PK), and (**c**) interleukin 18 (IL-18) models and how they are related. Solid arrows describe mass transfers, mixed dashed and dotted arrows relate to the effect compartment, and dashed arrows represent the statistically identified effects. The PK of atezolizumab was described by a two-compartment model. The timecourse of circulating IL-18 in plasma was described by the indirect response model, linked to a pool compartment. The increased IL-18 concentration was stimulated by an effect compartment concentration of atezolizumab. The changes in tumor size (sum of longest diameter (SLD)) were related to the atezolizumab area under the curve (AUC), and the relative change from baseline $(RCFB)_{IL\text{-}18,d21}$ (IL-18 RCFB at day 21). CL, clearance; V_c, central volume of distribution; Q, intercompartmental clearance; V_p, peripheral volume. R_{in}, zero-order input rate; k_{out}, first-order fractional turn-over rate constant; $Pool_0$, baseline concentration in the pool compartment; Slope, parameter related to the linear drug effect; k_{e0}, first-order effect compartment rate constant. R_{Growth} is the zero-order tumor growth rate, $K_{Shr,Drug}$, the tumor shrinkage rate constant related to drug AUC; and $K_{Shr,\ IL\text{-}18}$ tumor shrinking rate constant related to drug IL-18, respectively, λ_{Drug}, the rate constant describing the diminishing effect of AUC on tumor shrinkage with time.

the presence of liver metastases typically corresponds to larger disease burden, faster tumor growth, and worse treatment outcome.[37] Interestingly, current or former smokers were predicted to have a better drug response to atezolizumab than nonsmokers, whose tumor shrinkage rates were estimated to be reduced in early cycles of treatment compared to smokers. The model estimates that tumor shrinkage in nonsmokers is predominantly driven by the IL-18-related effect, whereas the AUC-related drug effect was not significantly different from zero ($K_{Shr,Drug} = 0$). This is consistent with the expectation of a higher tumor mutational load in smokers resulting in better immune recognition and, hence, an enhanced drug effect.

Future work includes external model validation, which was not feasible at the time of the analysis as additional clinical trials did not collect patient-level data for IL-18 for atezolizumab. A limitation of our analysis is that, although SLD is a well-accepted measure of tumor burden, it is a two-dimensional approximation of tumor volume and does not reflect the total disease burden. Technology, such as 3D positron emission tomography imaging,[38] may offer a better approximation of total disease burden for future TGI modeling. A key advantage of the framework described here is its ability to assess multiple factors systematically, taking into account the intersubject variability of various responses and leveraging the full temporal dynamics of the biomarker and tumor size data, resulting in further insights into patient-level responses. Future research in biomarker discovery and characterization may benefit from such an integrated approach based on a pharmacometric framework that enables an effective "learn and confirm" cycle, with the goal of informing dose and patient selection and ultimately optimizing patient outcomes in personalized medicine (**Figure 5**).

METHODS

Patients and data

Serum concentrations of atezolizumab and 95 plasma immunological biomarkers (**Table S1**) were analyzed in 88 patients with relapsed/refractory NSCLC in a first-in-human, dose-escalation phase I study, PCD4989g.[6] Tumor size was assessed by the RECIST trial[39] and SLD as measured by computed tomography. A summary of the dose administration, biomarker and PK sampling, and tumor assessment schedules is presented in **Table 2**. Additional baseline tumor biomarkers evaluated include: PD-L1 expression as assessed by immunohistochemistry; myeloid gene signature; gene expression levels of *MICB* and *MICA* genes, as assessed using a Fluidigm-based gene expression platform[6]; and epidermal growth factor receptor mutation status (**Table S6**).

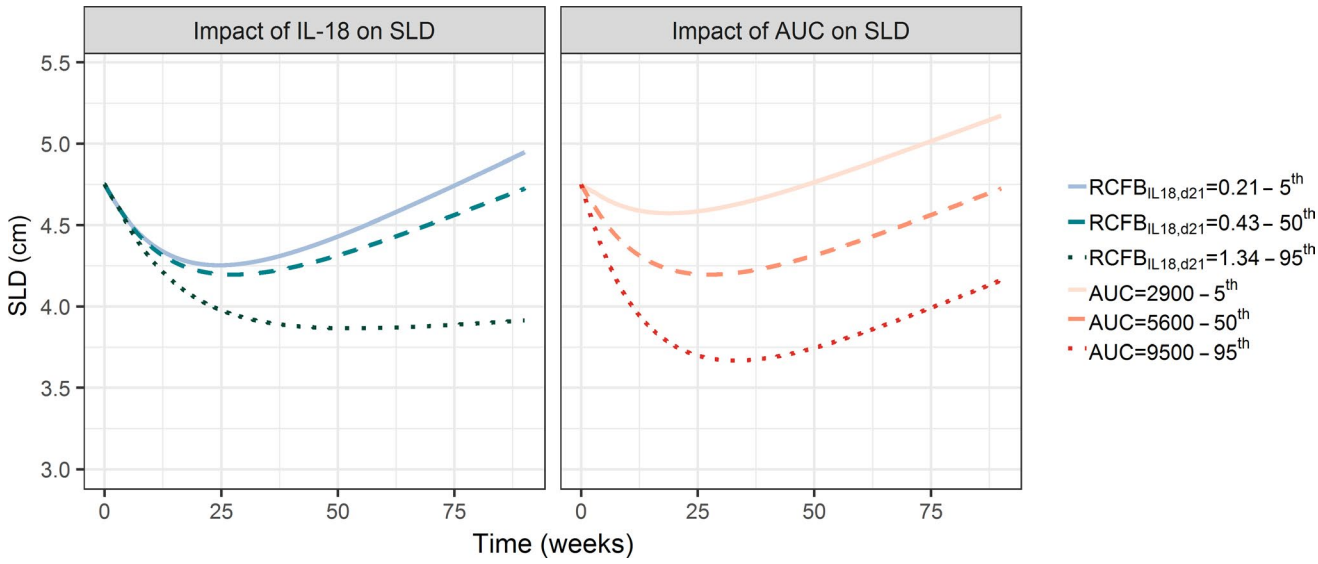

Figure 4 Simulations of the sum of the longest diameters (SLDs) timecourse for a typical patient (former/current smoker, has two or less metastases at baseline, and no liver metastases at baseline) to illustrate the impact of interleukin (IL)-18 (relative change in IL-18 from baseline at day 21 ($RCFB_{IL})_{-18,d21}$; left panel) or area under the curve (AUC) (right panel) on the tumor dynamics. *Left panel:* Simulations based on the 5th percentile (solid line), median (dashed line), and 95th percentile (dotted line) values of $RCFB_{IL-18,d21}$ and an AUC of 5,600 mg/l*day. *Right panel:* Simulates based on the 5th percentile (solid line), median (dashed line), and 95th percentile (dotted line) values of patient clearance and associated AUC values, and a typical $RCFB_{IL-18,d21}$ of 0.43.

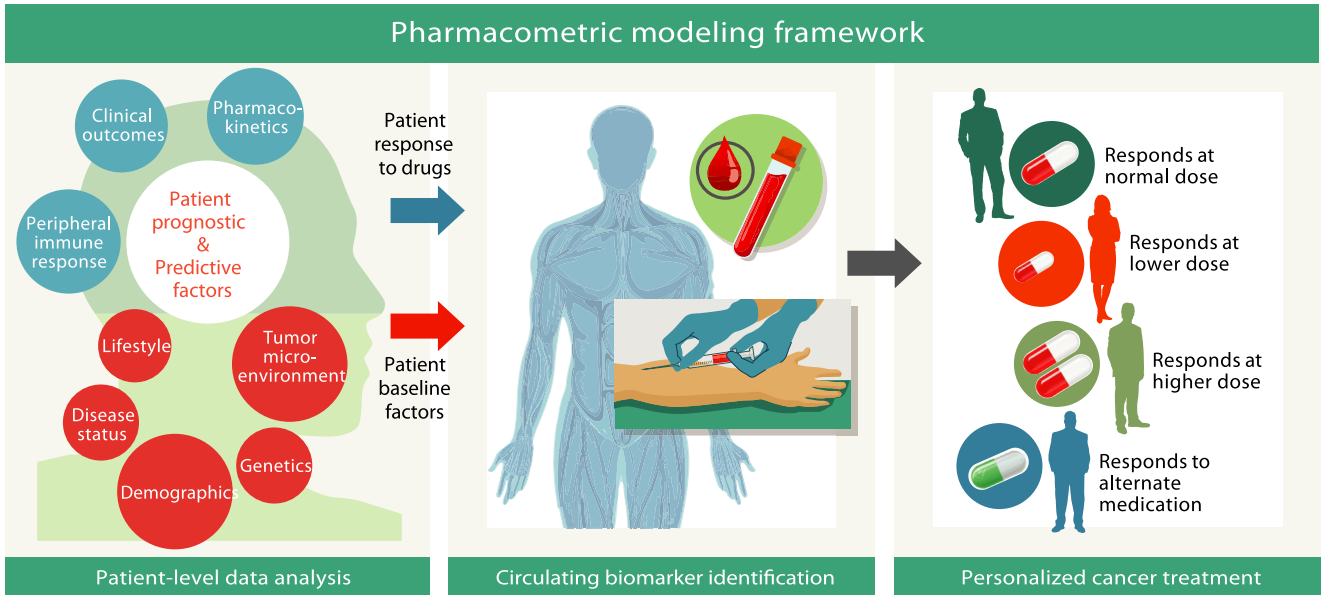

Figure 5 Schematic representation of a flexible, quantitative pharmacometric modeling framework to integrate multidimensional patient-level data to inform the identification of circulating predictive biomarkers for the ultimate goal of personalized cancer treatment.

Exploratory analyses to support biomarker selection for PK/PD tumor modeling

In order to streamline the modeling efforts, a screening procedure was conducted to prioritize the biomarkers of interest for PK/PD tumor modeling from the 95 plasma biomarkers collected, as described previously by Herbst *et al.*[6] Ten of the 95 showed statistically significant (P value ≤ 0.05) on-treatment changes from baseline levels (**Table S1**), among which five were considered biologically relevant as proximal markers to the mechanism of action of atezolizumab: CD40, ICAM-1, ITAC, IL-8, and VCAM-1. Additionally, CRP, IL-18, and $T_{CD8,prolif/activ}$ were prioritized based on scientific interest and biological relevance. These eight prioritized plasma markers were then further evaluated by graphical exploratory analysis and inspected for biomarker response in relation to atezolizumab exposure and changes in tumor size. The intrapatient and interpatient variability in the biomarker response, as well as potential complementary information (i.e., lack of strong between-biomarker correlations) by the different biomarkers, were evaluated through visual inspections of the individual and group-averaged response-time profiles.

Table 2 Summary of dosing, PK, and biomarker sampling as well as tumor size assessment schedules in patients with NSCLC in the PCD4989g study

Dosing and sampling/ assessment	Description
Dosing schedule	30–60 min I.V. infusion of atezolizumab every 3 weeks
Dosage	10–20 mg/kg or a fixed dose of 1,200 mg* *1 patient received 16 cycles of 1 mg/kg doses
PK sampling schedule[a]	Predose in cycles 1–8, 10, 12, 14–16, and ≥17; 30 minutes after end of infusion in cycles 1–7; 1, 3, 7, and 14 days after end of infusion in cycle 1
Biomarker sampling schedule	
All biomarkers (except $T_{CD8,prolif/activ}$)[b]	Predose in cycles 1–4 and 7; 30 minutes, 1 day and 7 days after end of infusion in cycle 1
$T_{CD8,prolif/activ}$	Predose in cycle 1–3 and 5
Tumor assessment schedule	Every 6 weeks for 24 weeks and every 12 weeks thereafter until disease progression, death, or further systemic cancer therapy

NSCLC, non-small cell lung cancer; PK, pharmacokinetic; $T_{CD8,prolif/activ}$, activated and proliferating CD8 T cells.
[a]The PK sampling scheduled varied for patients allocated to dose expansion or dose escalation cohorts. [b]"All biomarkers except $T_{CD8,prolif/activ}$" were: C-reactive protein, CD40 antigen, intercellular adhesion molecule 1, interferon-inducible T-cell alpha chemoattractant, interleukin 18, interleukin 8, and vascular cell adhesion molecule 1.

Following exploratory analyses, these eight biomarkers were studied in the final analyses of nonlinear mixed effect modeling.

PK model for atezolizumab

The PK of atezolizumab was described by a fit-for-purpose, two-compartment population PK model with dose-linear elimination, developed on data from 167 patients in the PCD4989g study who received doses of 10, 15, and 20 mg/kg every 3 weeks. The model *post hoc* estimates were used to derive cycle-specific $AUC_{cycle\ n}$ for the 88 patients with NSCLC according to Eq. 2:

$$AUC_{cycle\ n} = \frac{Dose_n}{CL_i} \quad (2)$$

where $Dose_n$ is the dose administered in cycle n and CL_i is the individual (empirical Bayes) estimate of clearance. In addition, AUC_{cycle1} was computed based on PK data from cycle 1 and tested as an alternative PK metric for correlation with antitumor response due to the low level of time-varying PK of atezolizumab (US Prescribing information, 2018). Parameter estimates are presented in **Table S3**.

Biomarker model

The change in biomarker concentration (BioM) in response to atezolizumab over time was evaluated by an IDR model[40] with a zero-order input rate (R_{in}) and a first-order fractional turnover rate constant (k_{out}), where the BioM at baseline ($BioM_0$) is the ratio between R_{in} (estimated) and k_{out} (estimated). Linear and saturable (E_{max} model) drug effect (EFF) models were evaluated. An E_{max} model did not provide a statistically better fit ($P > 0.01$) than the linear effect model. A dampening of the response over time was evaluated by linking a pool compartment (e.g., precursor of the biomarker) to the IDR model (Eq. 3)[41]:

$$\begin{aligned} \frac{dBioM_{pool}}{dt} &= R_{in} - k_{rel} \cdot BioM_{pool} \cdot (1 + EFF) \\ \frac{dBioM}{dt} &= k_{rel} \cdot BioM_{pool} \cdot (1 + EFF) - k_{out} \cdot BioM \\ k_{rel} &= k_{out} \cdot \frac{BioM_0}{BioM_{pool,0}} \end{aligned} \quad (3)$$

where $BioM_{pool}$ is the biomarker concentration in the pool compartment, k_{rel} is the first-order rate constant for the release of biomarker from the pool to plasma, and $BioM_{pool,0}$ (estimated) is the biomarker concentration in the pool compartment at baseline. The effect compartment model is described in Eq. 4:

$$\frac{dCE}{dt} = k_{e1} \cdot C_{atezolizumab} - k_{e0} \cdot CE \quad (4)$$

where CE is the effect compartment concentration of atezolizumab, k_{e1} and k_{e0} are two first-order effect compartment rate constants (here; $k_{e1} = k_{e0}$, estimated) and $C_{atezolizumab}$ is the PK model predicted atezolizumab concentration in the central compartment. The initial condition of CE was set to zero.

The observed baseline tumor size (SLD_0) was evaluated as a potential covariate for the production (R_{in}) of IL-18 and ITAC but was not significant (change in the OFV, ΔOFV, of 0.40 and 0.13, respectively).

A sequential method, the population PK parameters and data method,[42] was applied to estimate the PD parameters.

Tumor growth inhibition model

Change in tumor size was evaluated in three different structural TGI models.[21,31,43] Both exponential and linear[23,44] growth rate models were evaluated. Dose and drug exposure (i.e., AUC, Eq. 2) and model-based metrics of the biomarkers, including biomarker concentration over time (BM(t)), CFB, relative change from baseline at days 21 ($RCFB_{BM,d21}$) and 42 ($RCFB_{BM,d42}$), and cumulative AUC from baseline ($AUC_{BM,0\text{-}t}$) for IL-18 and ITAC, were evaluated for effect on the tumor shrinkage rate. Additionally, the RCFB at days 21 and 42, corresponding to peak levels of biomarkers, were evaluated as potential early metrics of response. An exponential decay in the AUC or biomarker effect on tumor shrinkage was investigated, as well as inclusion of an effect compartment. $RCFB_{BM,d21}$ and $RCFB_{BM,d42}$ were predicted for each individual from the biomarker models and set to zero before day 21 and day 42, respectively.

A covariate analysis was performed using the stepwise-covariate model building tool with P value < 0.01 level and P value < 0.001 level for forward selection and backward elimination, respectively. All explored parameter-covariate relationships are given in **Table S6**. Continuous covariates were included as power models and categorical covariates as a percentage of an effect relative to a reference category. The PD-L1 expression level was evaluated as a categorical covariate (i.e., PD-L1-high defined as immunohistochemistry of immune cell category 3 or immunohistochemistry of immune tumor cell category 3 vs. all other categories) in the TGI model. Nine patients (~10%) did not have known PD-L1 expression values due to insufficient tumor contents from the collected biopsy samples and were excluded from the covariate analysis when PD-L1 expression was evaluated (**Table S5**).

A time-to-event model for dropouts was developed for model evaluation by VPC and to avoid potential bias in the simulated tumor size in comparison to clinical trial observations. A dropout event was assumed to occur 3 weeks after the last tumor observation time. The baseline hazard ($h_0(t)$) was evaluated as an exponential and as a Weibull distribution. Potential predictors of dropout were explored, alone and in combination,

on the hazard ($h(t)$), Eq. 5:

$$h(t) = h_0(t) \cdot e^{\beta_1 \cdot x_1 + \beta_2 \cdot x_2} \quad (5)$$

where β1 and β2 are parameters describing the effect of the predictors x_1 and x_2.

Model simulation of AUC and IL-18 effect on tumor size

The tumor size kinetic profile for a reference patient with NSCLC (two or less metastases at baseline, no liver metastases at baseline, and former/current smoker) given a fixed dose of 1,200 mg atezolizumab was simulated. Three different values corresponding to the 5th, 50th, and 95th percentiles of estimated AUC and the $RCFB_{IL\text{-}18,d21}$, respectively, were used in the simulations.

Model development

The first-order conditional estimation method with interaction and the Laplacian estimation method were used for parameter estimation for the biomarker, and tumor size and the dropout models using NONMEM version 7.3.[45] Data management, graphical evaluation, and further processing of the NONMEM output were performed using R software version 3.1.2 (https://www.R-project.org). The Perl-speaks-NONMEM toolkit version 4 was used to execute model runs and automate processes, such as VPCs, and to perform covariate model building.[46] The R-based packages Xpose version 4 and ggplot2 version 1.0.0 (www.ggplot2.org) were used for model diagnosis and graphical explorations. Simulations based on the different biomarker variable values were performed in Berkeley Madonna.[47]

Discrimination between models was primarily based on inspection of graphical diagnostics and changes in the OFV (i.e., −2 × log-likelihood) using the likelihood ratio test. Given that models are nested, the ΔOFVs are nominally χ^2 distributed and the additional number of parameters (larger to smaller model) is the degree of freedom. A P value of < 0.01 was used for significance testing. VPCs and pcVPCs[48] were generated to evaluate the predictive performance of the models, given the observed data.

The data were log-transformed and the residual error was modeled as being additive and proportional for the ITAC model, but proportional for the IL-18 and TGI models on the log-scale. Other error models were explored when misspecification was indicated based on the graphical diagnostics. Interindividual variability was assumed to be log-normally distributed with a mean of 0 and a variance of ω^2.

SUPPORTING INFORMATION

Additional supporting information may be found in the online version of this article on the *Clinical Pharmacology & Therapeutics* website (www.cpt-journal.com).

Figure S1. The relative change in biomarker level from baseline (at day 21) vs. the relative change in tumor size from baseline (at the end of cycle 6) for the eight evaluated biomarkers.

Figure S2. Prediction corrected visual predictive check (pcVPC) of the population pharmacokinetic (PK) model for atezolizumab applied to the 88 patients with non-small cell lung cancer, where the structural parameters were estimated as: clearance (CL), 0.233 l/day; volume of distribution (*Vc*), 3.35 l; intercompartmental clearance (*Q*), 0.452 l/day; peripheral volume of distribution (*Vp*), 3.36 l.

Table S1. Peripheral biomarkers ($n = 95$) evaluated using Rules Based Medicine (Myriad RBM), MESO Scale Discovery (MSD), and fluorescence-activated cell sorter (FACS) panels.

Table S2. Number of observations above the limit of quantification (LOQ) and tumor size assessments.

Table S3. Final parameter estimates and relative standard errors (RSE) for the population PK model.

Table S4. Summary of objective function values (OFVs) of selected tumor growth inhibition (TGI) models evaluated with different predictors of tumor shrinkage.

Table S5. Summary statistics of baseline covariates evaluated during the TGI model development.

Table S6. Parameter-covariate relationships explored in the covariate analysis.

ACKNOWLEDGMENTS

The authors thank Mahrukh Huseni, Jin Jin, Ina Rhee, Yuan-Yuan Xiao, Jeong Kim, and Eric Stefanich for their helpful input on the project and analyses and the Genentech DTECT committee for providing funding. The authors would also like to acknowledge Anshin Biosolutions for providing publication support, funded by Development Sciences in Genentech Research and Early Development (gRED).

FUNDING

This study was funded by Genentech.

CONFLICT OF INTEREST

C.C.L., N.R.B., L.M., and S.S. are employees of Genentech, Inc., and stockholders of the Roche group. I.N., E.N.J., and L.E.F. were paid consultants working with Genentech during the PK/PD analysis.

AUTHOR CONTRIBUTIONS

C.C.L., I.N., L.M., E.N.J., M.S., N.R.B., S.S., and L.E.F. wrote the manuscript. C.C.L, L.M., I.N., and L.E.F. designed the research. I.N., C.C.L., L.M., M.S., E.N.J., N.R.B., S.S., and L.E.F. performed the research. I.N., C.C.L, and L.E.F. analyzed the data.

1. Schadendorf, D. *et al.* Pooled analysis of long-term survival data from phase II and phase III trials of ipilimumab in unresectable or metastatic melanoma. *J. Clin. Oncol.* **33**, 1889–1894 (2015).
2. Garon, E.B. *et al.* Pembrolizumab for the treatment of non-small-cell lung cancer. *N. Engl. J. Med.* **372**, 2018–2028 (2015).
3. Powles, T. *et al.* MPDL3280A (anti-PD-L1) treatment leads to clinical activity in metastatic bladder cancer. *Nature* **515**, 558–562 (2014).
4. Chen, D.S. & Mellman, I. Oncology meets immunology: the cancer-immunity cycle. *Immunity* **39**, 1–10 (2013).
5. Chen, D.S. & Mellman, I. Elements of cancer immunity and the cancer-immune set point. *Nature* **541**, 321–330 (2017).
6. Herbst, R.S. *et al.* Predictive correlates of response to the anti-PD-L1 antibody MPDL3280A in cancer patients. *Nature* **515**, 563–567 (2014).
7. Fehrenbacher, L. *et al.* Atezolizumab versus docetaxel for patients with previously treated non-small-cell lung cancer (POPLAR): a multicentre, open-label, phase 2 randomised controlled trial. *Lancet* **387**, 1837–1846 (2016).
8. Sul, J., Blumenthal, G.M., Jiang, X., He, K., Keegan, P. & Pazdur, R. FDA approval summary: pembrolizumab for the treatment of patients with metastatic non-small cell lung cancer whose tumors express programmed death-ligand 1. *Oncologist* **21**, 643–650 (2016).
9. Morrissey, K.M., Yuraszeck, T.M., Li, C.C., Zhang, Y. & Kasichayanula, S. Immunotherapy and novel combinations in

oncology: current landscape, challenges, and opportunities. *Clin. Transl. Sci.* **9**, 89–104 (2016).
10. Spranger, S. & Gajewski, T. Rational combinations of immunotherapeutics that target discrete pathways. *J. Immunother. Cancer* **1**, 16 (2013).
11. Cha, E., Wallin, J. & Kowanetz, M. PD-L1 inhibition with MPDL3280A for solid tumors. *Semin. Oncol.* **42**, 484–487 (2015).
12. Grigg, C. & Rizvi, N.A. PD-L1 biomarker testing for non-small cell lung cancer: truth or fiction? *J. Immunother. Cancer* **4**, 48 (2016).
13. Gulley, J.L. *et al.* Role of antigen spread and distinctive characteristics of immunotherapy in cancer treatment. *J. Natl. Cancer Inst.* **109**, (2017).
14. Lawrence, M.S. *et al.* Mutational heterogeneity in cancer and the search for new cancer-associated genes. *Nature* **499**, 214–218 (2013).
15. Kelderman, S. *et al.* Lactate dehydrogenase as a selection criterion for ipilimumab treatment in metastatic melanoma. *Cancer Immunol. Immunother.* **63**, 449–458 (2014).
16. Wilgenhof, S. *et al.* Single-center experience with ipilimumab in an expanded access program for patients with pretreated advanced melanoma. *J. Immunother.* **36**, 215–222 (2013).
17. Yuan, J. *et al.* Pretreatment serum VEGF is associated with clinical response and overall survival in advanced melanoma patients treated with ipilimumab. *Cancer Immunol. Res.* **2**, 127–132 (2014).
18. Carthon, B.C. *et al.* Preoperative CTLA-4 blockade: tolerability and immune monitoring in the setting of a presurgical clinical trial. *Clin. Cancer Res.* **16**, 2861–2871 (2010).
19. Gebhardt, C. *et al.* Myeloid cells and related chronic inflammatory factors as novel predictive markers in melanoma treatment with ipilimumab. *Clin. Cancer Res.* **21**, 5453–5459 (2015).
20. Hannani, D. *et al.* Anticancer immunotherapy by CTLA-4 blockade: obligatory contribution of IL-2 receptors and negative prognostic impact of soluble CD25. *Cell Res.* **25**, 208–224 (2015).
21. Chatterjee, M. *et al.* Systematic evaluation of pembrolizumab dosing in patients with advanced non-small-cell lung cancer. *Ann. Oncol.* **27**, 1291–1298 (2016).
22. Bender, B.C., Schindler, E. & Friberg, L.E. Population pharmacokinetic-pharmacodynamic modelling in oncology: a tool for predicting clinical response. *Br. J. Clin. Pharmacol.* **79**, 56–71 (2015).
23. Wang, Y. *et al.* Elucidation of relationship between tumor size and survival in non-small-cell lung cancer patients can aid early decision making in clinical drug development. *Clin. Pharmacol. Ther.* **86**, 167–174 (2009).
24. Claret, L., Lu, J.F., Sun, Y.N. & Bruno, R. Development of a modeling framework to simulate efficacy endpoints for motesanib in patients with thyroid cancer. *Cancer Chemother. Pharmacol.* **66**, 1141–1149 (2010).
25. Hansson, E.K. *et al.* PKPD modeling of predictors for adverse effects and overall survival in sunitinib-treated patients with GIST. *CPT Pharmacometrics Syst. Pharmacol.* **2**, e85 (2013).
26. Schindler, E., Amantea, M.A., Karlsson, M.O. & Friberg, L.E. PK-PD modeling of individual lesion FDG-PET response to predict overall survival in patients with sunitinib-treated gastrointestinal stromal tumor. *CPT Pharmacometrics Syst. Pharmacol.* **5**, 173–181 (2016).
27. van Hasselt, J.G., Gupta, A., Hussein, Z., Beijnen, J.H., Schellens, J.H. & Huitema, A.D. Integrated simulation framework for toxicity, dose intensity, disease progression, and cost effectiveness for castration-resistant prostate cancer treatment with eribulin. *CPT Pharmacometrics Syst. Pharmacol.* **4**, 374–385 (2015).
28. Schindler, E., Amantea, M.A., Karlsson, M.O. & Friberg, L.E. A pharmacometric framework for axitinib exposure, efficacy, and safety in metastatic renal cell carcinoma patients. *CPT Pharmacometrics Syst. Pharmacol.* **6**, 373–382 (2017).
29. Hansson, E.K. *et al.* PKPD modeling of VEGF, sVEGFR-2, sVEGFR-3, and sKIT as predictors of tumor dynamics and overall survival following sunitinib treatment in GIST. *CPT Pharmacometrics Syst. Pharmacol.* **2**, e84 (2013).
30. Stroh, M. *et al.* Clinical pharmacokinetics and pharmacodynamics of atezolizumab in metastatic urothelial carcinoma. *Clin. Pharmacol. Ther.* **102**, 305–312 (2017).
31. Claret, L. *et al.* Model-based prediction of phase III overall survival in colorectal cancer on the basis of phase II tumor dynamics. *J. Clin. Oncol.* **27**, 4103–4108 (2009).
32. Zaretsky, J.M. *et al.* Mutations associated with acquired resistance to PD-1 blockade in melanoma. *N. Engl. J. Med.* **375**, 819–829 (2016).
33. Rittmeyer, A. *et al.* Atezolizumab versus docetaxel in patients with previously treated non-small-cell lung cancer (OAK): a phase 3, open-label, multicentre randomised controlled trial. *Lancet* **389**, 255–265 (2017).
34. Novick, D., Kim, S., Kaplanski, G. & Dinarello, C.A. Interleukin-18, more than a Th1 cytokine. *Semin. Immunol.* **25**, 439–448 (2013).
35. Harris, S.J., Brown, J., Lopez, J. & Yap, T.A. Immuno-oncology combinations: raising the tail of the survival curve. *Cancer Biol. Med.* **13**, 171–193 (2016).
36. Bruno, R., Claret, L., Marchand, M. & Jin, J. Tumor growth rate – OS models inform drug development decisions. In FDA-AACR Oncology Dose Finding Worksop, Part 3.
37. Tamura, T. *et al.* Specific organ metastases and survival in metastatic non-small-cell lung cancer. *Mol. Clin. Oncol.* **3**, 217–221 (2015).
38. Schindler, E., Krishnan, S.M., Mathijssen, R., Ruggiero, A., Schiavon, G. & Friberg, L.E. Pharmacometric modeling of liver metastases' diameter, volume, and density and their relation to clinical outcome in imatinib-treated patients with gastrointestinal stromal tumors. *CPT Pharmacometrics Syst. Pharmacol.* **6**, 449–457 (2017).
39. Eisenhauer, E.A. *et al.* New response evaluation criteria in solid tumours: revised RECIST guideline (version 1.1). *Eur. J. Cancer* **45**, 228–247 (2009).
40. Dayneka, N.L., Garg, V. & Jusko, W.J. Comparison of four basic models of indirect pharmacodynamic responses. *J. Pharmacokinet. Biopharm.* **21**, 457–478 (1993).
41. Movin-Osswald, G. & Hammarlund-Udenaes, M. Prolactin release after remoxipride by an integrated pharmacokinetic-pharmacodynamic model with intra- and interindividual aspects. *J. Pharmacol. Exp. Ther.* **274**, 921–927 (1995).
42. Zhang, L., Beal, S.L. & Sheiner, L.B. Simultaneous vs. sequential analysis for population PK/PD data I: best-case performance. *J. Pharmacokinet. Pharmacodyn.* **30**, 387–404 (2003).
43. Simeoni, M. *et al.* Predictive pharmacokinetic-pharmacodynamic modeling of tumor growth kinetics in xenograft models after administration of anticancer agents. *Cancer Res.* **64**, 1094–1101 (2004).
44. Li, C.H. *et al.* Comparative effects of CT imaging measurement on RECIST end points and tumor growth kinetics modeling. *Clin. Transl. Sci.* **9**, 43–50 (2016).
45. Beal, S., Sheiner, L.B., Boeckmann, A. & Bauer, R.J. *NONMEM User's Guides (1989-2009)* (Icon Development Solutions, Ellicott City, MD, 2009).
46. Keizer, R.J., Karlsson, M.O. & Hooker, A. Modeling and simulation workbench for NONMEM: tutorial on Pirana, PsN, and Xpose. *CPT Pharmacometrics Syst. Pharmacol.* **2**, e50 (2013).
47. Macey, R., Oster, G. & Zahnley, T. Berkeley Madonna Users Guide. <https://mcb.berkeley.edu/courses/mcb137/exercises/madonnamanual.pdf> (2003). Accessed 3 September 2017.
48. Bergstrand, M., Hooker, A.C., Wallin, J.E. & Karlsson, M.O. Prediction-corrected visual predictive checks for diagnosing nonlinear mixed-effects models. *AAPS J.* **13**, 143–151 (2011).